Catalysis Today 413-415 (2023) 113945

Contents lists available at ScienceDirect

Catalysis Today

journal homepage: www.elsevier.com/locate/cattod

H_2 production by cellulose photoreforming with TiO_2-Cu photocatalysts bearing different Cu species

Sergio Belda-Marco, Maria Angeles Lillo-Ródenas, Maria Carmen Román-Martínez *

MCMA Group, Department of Inorganic Chemistry and Materials Institute (IUMA), University of Alicante, E-03080 Alicante, Spain

ARTICLE INFO

Keywords:
Titanium dioxide
Copper
Hydrogen
Cellulose
Photocatalysis

ABSTRACT

TiO_2-Cu photocatalysts (1 wt% Cu) containing different copper species have been prepared and used for the generation of hydrogen by photoreforming of cellulose (the major component of biomass) in water at room temperature using UV light. A positive effect of copper has been clearly observed, and the analysis of the role of the Cu species present shows that a mixture of Cu(I) and Cu(II) favors the process. Among the TiO_2-Cu photocatalysts, the one prepared by a simple impregnation method and not heat-treated, which shows small and well dispersed copper species particles, gives the highest hydrogen production.

1. Introduction

The current energy model based on fossil fuels has led to the accumulation of CO_2 in the atmosphere, with the known greenhouse effect and global warming [1]. The associated negative environmental effects are impelling the decarbonization of the energy and mobility fields. A way to reduce CO_2 emissions is the substitution of fossil fuels by energy sources with no (or less) CO_2 footprint and, in this context, H_2 can be considered the cleanest fuel if its production is based on renewable and non-polluting sources. It is possible to address this challenge using suitable catalysis technologies. Among them, photocatalysis has shown to be able to contribute to the production of hydrogen and high added-value hydrocarbons. This can occur by means of the effective transformation of abundant or renewable resources like biomass residues, water, and sunlight through the process known as photoreforming [2–5].

Lignocellulosic biomass is usually the surplus of naturally produced organic matter, ranging from agriculturally grown crops to wood wastes, such as pellets or sawdust. In general, it is composed (on a dry weight basis) of 75% carbohydrates (cellulose and hemicellulose) and 10–20 % lignin, being the rest lipids. Cellulose, the major component and the most easily degradable one [3], is a linear crystalline polymer consisting of glucose units linked by β(1−4) glycosidic bonds that can be represented by the chemical formula $(C_6H_{12}O_5)_n$. It has a complex and stable structure, difficult to degrade, resulting from an extensive network of intramolecular and intermolecular hydrogen bonds.

Cellulose photoreforming can be envisaged by Eq. 1, although degradation products of cellulose can be formed instead of CO_2.

$$(C_6H_{10}O_5)n + 7nH_2O \rightarrow 6nCO_2 + 12nH_2 \quad (1)$$

A photocatalyst is basically a semiconductor that becomes activated by UV or visible light, depending on the band gap, generating e^-/h^+ (electron/holes) pairs [3,4]. The charge carriers can reach the semiconductor surface and participate in interphase redox reactions. The basic and simplified set of reactions of cellulose photoreforming is the following [6,7]:

1. $semiconductor + hv \rightarrow e^- + h^+$
2. $H_2O \rightarrow OH^- + H^+$
3. $e^- + H^+ \rightarrow \frac{1}{2}H_2$
4. $h^+ + H_2O \rightarrow OH^{\cdot} + H^+$
5. $HO^{\cdot} + Cellulose \rightarrow Glucose$
6. $HO^{\cdot} + Glucose \rightarrow e^- + h^+ + CO_2$

In this scheme, glucose represents also other potential degradation product of cellulose (such as galactose, arabinose, rhamnose, xylose, mannose, etc.,).

Titanium dioxide is an effective photocatalyst, widely used because it is chemically, physically, and thermally stable, non-toxic, and relatively inexpensive [8,9]. However, it has some disadvantages, such as a high e^-/h^+ recombination rate and relatively high band gap (UV light is required). These drawbacks can be overcome by combining TiO_2 with other substances, like, for example, transition metals, non-metallic

* Corresponding author.
E-mail address: mcroman@ua.es (M.C. Román-Martínez).

https://doi.org/10.1016/j.cattod.2022.11.006
Received 29 August 2022; Received in revised form 18 October 2022; Accepted 3 November 2022
Available online 4 November 2022

elements, dyes, surface functionalities, etc. [10–15]. Such additives can either facilitate the transfer of charge carriers to hinder their recombination, leading to a modification of the host material band gap (including the creation of new electronic states), or to make the light harvesting more efficient. Also, some metals or metal compounds can be semiconductors, with the subsequent potential creation of heterojunctions, or they can act as co-catalysts of the target reaction.

The first studies to produce hydrogen by hydrocarbons photoreforming (Kawai and Sakata [16]) used a physical mixture of TiO_2, RuO_2 and Pt. Later, different methods have been used to incorporate metals to TiO_2 and the target has become to replace noble metals by non-noble metals such as Ni, Cu, and Co [17–20]. Among them, copper and copper oxides are interesting because they are good electrical conductor and semiconductor of smaller band gap than TiO_2, respectively. However, there is controversy about which copper species are the most effective to improve the properties of TiO_2 for this reaction. Considering this, the present work focuses on the preparation of TiO_2-Cu catalysts by different methods to obtain photocatalysts with copper in different oxidation states able to generate hydrogen by cellulose photoreforming.

2. Experimental

2.1. Synthesis of photocatalysts

Titania P25 (Degussa, 70–80 % anatase and 30–20 % rutile) has been used to prepare Cu-TiO_2 photocatalysts. Its average crystallite and particle size are, respectively, 25 nm and 0.1 μm [21,22], and the specific surface area is around 50 m^2/g [22].

Cu-P25 catalysts (nominal 1 wt% Cu) have been prepared by the following procedures:

-Wet impregnation. Dried P25 (3 g) and deionized water (15 mL) are magnetically stirred (10 min). Then, a $Cu(NO_3)_2 \cdot 3\,H_2O$ aqueous solution (30 mL) is added, and the mixture is ultrasonicated (20 min) and placed in an oil bath (35 °C, 7 h) under magnetic stirring. Afterwards, the mixture is ultrasonicated again (20 min) and then, transferred to a crystallizer, and dried at 80 °C for 15 h. Procedure adapted from references [18,23]. Sample named P25-Cu-i.

-Wet impregnation + calcination. Sample P25-Cu-i is heat treated as follows: 3 °C/min up to 150 °C, 2 h soaking time, and 5 °C/min up to 500 °C, 1 h soaking time. Sample named P25-Cu-ic.

-Wet impregnation + reduction with H_2. Sample P25-Cu-i is reduced inside a U-shaped quartz reactor (H_2 flow (60 mL/min) 500 °C (heating rate 5 °C/min), 2 h). The catalyst, named P25-Cu-ih, is stored in a vial filled with Ar. After approximately one month, the inert atmosphere was not preserved and the sample turned light gray, being named P25-Cu-iht.

-Wet impregnation + calcination + reduction with H_2. Sample P25-Cu-ic is submitted to the reduction treatment described above. The resulting sample is called P25-Cu-ich and is also stored in Ar.

-Impregnation + reduction with $NaBH_4$. Titania P25 (3 g) is added to an aqueous solution (20 mL) of $Cu(NO_3)_2 \cdot 3\,H_2O$. The mixture is magnetically stirred (10 min) and placed in an ice-water bath. $NaBH_4$ (0.0193 g) is added and magnetic stirring is kept for 2 h. The solid is washed with ultrapure H_2O, and dried at 105 °C overnight (16 h). The preparation of this photocatalyst, named P25-Cu-ib, is based on the work of Xu et al. [24], who proposed that Cu_2O is formed in these conditions.

- Cu incorporation by ligand exchange. Starting with $Cu(NO_3)_2 \cdot 3\,H_2O$, several reactants are used to obtain an oxalate copper complex that is deposited on P25. The detailed description of the procedure is presented in the supplementary information, SI, accompanied by a photograph showing the color changes (Figure S1). Sample named P25-Cu-o.

2.2. Characterization of photocatalysts

The actual copper content (and Na content in some samples) in the catalysts was determined after extraction with aqua regia and analysis by ICP-OES (Perkin Elmer, model 7300 DV (dual vision)). Details on the procedure are included in the SI.

The band gap energy (E_g) of the photocatalysts was determined using 0.1 g sample and λ scan 800–200 nm (Jasco V-670 UV–vis spectrophotometer).

The photocatalysts were characterized by XRD (Miniflex II Rigaku (30 kV/15 mA)) with Cu K_α radiation (λ = 0.1540 nm), from 6° to 80° 2θ at 2°/min, XPS (Thermo-Scientific K-Alpha, 1486.6 eV Al K_α X-ray source), with a pass energy of 50 eV, and 0.1 eV scan step, irradiating 400 μm of the sample, binding energy (B.E.) values adjusted to the C1s transition (284.6 eV); and TEM (JEOL, JEM-2010 200 keV, with a GATAN ORIUS SC600 camera and GATAN Digital Micrograph 1.80.70 for GMS 1.8.0).

2.3. Catalytic activity tests

The experimental setup used for the catalytic activity tests consists of a glass photo reactor (Heraeus UV-RS-2) equipped with a medium-pressure mercury UV lamp (Heraeus TQ-150, undoped, 150 W, radiation flux (Φ) of 47 W in the 200–600 nm range and λ_{max} = 365 nm) that includes a built-in cooling system which allows maintaining the reaction temperature at 25 °C. The inlet gas (He) is driven to the lower part of the reactor, bubbling through the liquid. The outlet gas flows through a moisture trap before reaching the mass spectrometer (Balzers, OmniStar GSD 301 O1) (Figure S2).

In a typical experiment, 1 g ball-milled cellulose (milling described in SI), 20 mg photocatalyst, 500 mL distilled water, and a magnetic stirrer are introduced into the reactor. Then, the reactor, wrapped with an aluminum foil cover, is well purged with helium (60 mL/min) to displace any dissolved oxygen, and the lamp is switched on and kept on for 5 h.

The following "blank" experiments have been performed: 1) with cellulose but without catalyst (B1), 2) without cellulose and without catalyst (B2), and 3) without cellulose and using P25 (B3a), and without cellulose and using P25-Cu-i (B3b).

3. Results and discussion

3.1. Catalysts characterization

3.1.1. Visual analysis and ICP-OES results

The prepared photocatalysts show different colors, a clear indication of the different copper species developed (Fig S3).

Sample P25-Cu-i shows a pale greenish-blue color that can be attributed to a basic copper salt, which could have been formed either by hydrolysis of copper nitrate in water or by its partial decomposition during the catalyst drying at 80 °C [25]. Sample P25-Cu-ic looks brownish, and this color suggests the presence of Cu_2O and CuO. Samples P25-Cu-ih and P25-Cu-ich show a predominant indigo color that can be due to reduced titania with some contribution of the presence of Cu(I) and/or Cu(0) species, the last one also able to promote the coloration by the plasmonic effect [26,27]. Sample P25-Cu-iht looks gray-like, indicating the presence of Cu or CuO and, likely, also partially reduced titania. Sample P25-Cu-ib shows a quite pale gray-blue color, suggesting that partially reduced copper species are present. The sky-blue color of P25-Cu-o reveals that the coordination of copper is different from that in P25-Cu-i.

The Cu content (wt%) in the prepared catalysts determined by ICP-OES is very close to 1 wt% in all samples, except in P25-Cu-ib, which contains 0.5 wt% Cu (Table S3). In this case, the preparation procedure includes a final washing step that seems to have leached out part of the deposited Cu (in agreement with the very pale color (Figure S3)).

Sample P25-Cu-o contains a relatively high amount of Na (3.6 wt%), remaining from NaOH and $CH_3COONa{\cdot}3\ H_2O$ used in its preparation.

3.1.2. UV-Vis results

The UV-Vis absorbance spectra (Fig. 1a) reveal the important effect of the presence of copper in the optical properties of the P25-Cu photocatalysts. In the λ range 200–400 nm all samples present the high absorbance characteristic of P25, but the Cu-containing photocatalysts show additional features (relative maxima at 215 and 325 nm) that are likely related to LMCT (ligand to metal charge transfer) transitions involving O^{2-} and copper species [28]. Besides, the P25-Cu samples, particularly those analysed just after the reduction treatment with H_2 and kept in an inert atmosphere until the measurement, show significant absorbance above 400 nm. According to Schubert et al. [29] absorbance between 400 and 550 nm can be the result of: localized surface plasmon resonance (LSPR) of Cu(0) nanoparticles, Cu(0) d-s transitions, interfacial charge transfer from TiO_2 to Cu(II) and metal-to-ligand charge-transfer (MLCT) associated to Cu(I), while the strong absorption between 550 and 900 nm is due to d-d transitions in Cu(II) [29]. On the other hand, DeSario et al. attribute the absorption between 560 and 760 nm to LSPR [30]. Therefore, it can be stated that the H_2 heat treated samples contain Cu(0) and a strong LSPR, which is higher for the reduced sample that had not been previously calcined. For the rest of the samples, the absorbance profiles show differences in the 550–900 nm wavelength region, revealing a different role of the copper species, following the decreasing order of absorbance: P25-Cu-icht > P25-Cu-ic > P25-Cu-i > P25-Cu-ib > P25-Cu-o > P25. P25-Cu-i, P25-Cu-ic, and P25-Cu-ib present a very similar profile between 550 and 900 nm that reveal the presence of Cu(II) (absorbance due to d-d transitions), while the shape of the absorbance curve for P25-Cu-o suggests a LSPR effect and thus, the presence of Cu(0).

The complete set of calculated E_g values (by indirect K-M method (the most appropriate for the photocatalysts studied in this work [31])) is shown in Table S1.

The E_g values of the Cu-containing catalysts are lower than that of pure P25, and show some slight differences between them, revealing the effect of the different copper species present. The lower E_g values, 2.24 and 2.35 eV, correspond to samples reduced by treatment with hydrogen at high temperature (500 °C), catalysts P25-Cu-ih and P25-Cu-ich, respectively. For the sample calcined at 500 °C, P25-Cu-ic, and those reduced or prepared at room temperature, P25-Cu-ib, P25-Cu-o and P25-Cu-i, the values are significantly higher: 2.82, 2.91, 2.97 eV and 2.91 eV, respectively.

3.1.3. XRD results

The X-ray diffraction analysis of the prepared photocatalysts mainly shows the characteristic patterns of P25 [8,32,33], Figure S4. Peaks with very low intensity that could correspond to Cu species can be distinguished for some samples (marked in Figure S4). The main diffraction peaks of anatase, rutile, Cu and Cu oxides, collected in the JCPDS and JCPDF database, are included in Table S2. These data show the overlapping of some titania and copper species peaks (that totally affects the most intense reflection peaks of the copper species).

With the caution imposed by the low intensity of the Cu peaks and the mentioned overlapping, it can be stated that samples P25-Cu-iht, P25-Cu-o, and P25-Cu-ich contain Cu(0) or Cu_2O (peak at 2θ 74°). Besides, for these samples and for P25-Cu-i, peaks at 2θ 29.8 and 42.3°, corresponding to Cu_2O, seem to be present [34,35]. Assignment of CuO is not conclusive because the corresponding most intense peaks overlap with those of TiO_2. No peaks due to Cu species can be distinguished for sample P25-Cu-ib, may be related to the low metal loading, while for sample P25-Cu-o significantly different peaks are observed in the 30–35.5° 2θ range, which are attributed to Na species, likely NaOH, Na_2O or Na_2CO_3 [36–39].

3.1.4. XPS results

The Cu $2p_{3/2}$ XPS spectra obtained for the prepared P25-Cu samples (Fig. 1b) show a broad peak at B.E. from 930 to 938 eV that, in some cases, can be deconvoluted into two contributions (denoted as peak A and peak B). Peak A, at about 932.3 eV, is due to Cu(0) and/or Cu(I) [40, 41], while peak B, close to 934 eV, stands from more oxidized Cu species. Details on precise B.E. values, the relative contribution of A and B peaks, and surface Cu wt% are presented in Table S3.

The XPS analysis of supported species is complicated because the particle size and the interaction of those species with the support have a relevant influence on the position and shape of the peaks (width, satellite structure, etc.) of both, photoelectron and Auger signals [42]. Besides, in the case of supported copper, determining whether copper is present as Cu(0) or Cu(I) is complex since both species have similar binding energy.

For samples P25-Cu-i and P25-Cu-ic, peak B can be assigned to Cu(II) since satellite peaks (from 938 to 945 eV) are clearly observed in the spectra [40,42,43]. For samples P25-Cu-ich and P25-Cu-ib, peak B appears at 933.3 eV and no satellite peak is observed, meaning that either these samples do not contain Cu(II) or that the satellite peaks are not observable due to the very low amount of this species. For sample P25-Cu-o, the XPS signal has very low intensity, but it should be related to Cu(0) or Cu(I). The amount of surface Cu in this sample is noticeably lower than in the other catalysts, and a significant amount of sodium is

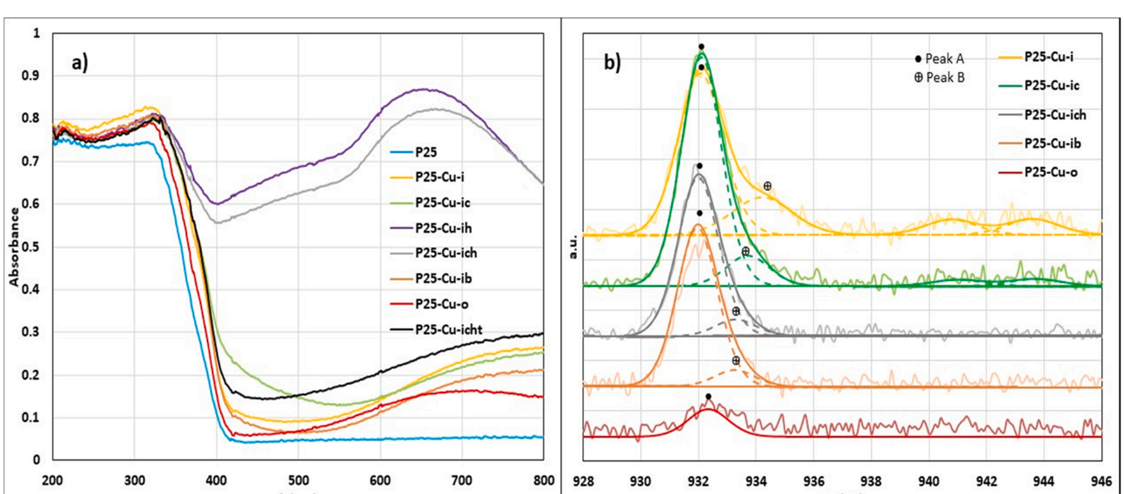

Fig. 1. **a)** Absorbance vs wavelength profiles of P25 and P25-Cu photocatalysts and **b)** Cu $2p_{3/2}$ XPS spectra for the P25-Cu catalysts.

detected (higher than the one determined by ICP) which could be partially covering copper species. In general, the photocatalysts show surface enrichment of copper species (revealed by the surface Cu wt%, higher than the total Cu loading, Table S3), being more marked in the case of the calcined samples.

As a summary, it can be stated that P25-Cu-i contains Cu(II) present as nitrate, hydroxide or oxide, and Cu(I) species (24 % and 76 %, respectively, of the total amount of detected Cu). P25-Cu-ic contains Cu (II) and Cu(I) (13 % and 87 %, respectively). Because of the preparation method, it is unlikely that Cu(0) is present in these two samples. P25-Cu-ich and P25-Cu-ib could contain a mixture of Cu(0) and Cu(I), and probably a small amount of Cu(II), and P25-Cu-o, likely contains Cu(0), that might be partially covered by Na species.

Analysis of the Auger electrons to distinguish Cu(0) or Cu(I) [42,43] is very difficult because the intense XPS Ti 2 s transition (565.3 eV) overlaps the Auger CuLMM one (567.6–573.6 eV) [44]. However, a thorough analysis of the Auger spectra shows slight but relevant differences between samples, and also with respect to analogous data obtained for P25 (Fig. 2). The main features in the Cu ($L_3M_{4,5}M_{4,5}$) Auger spectra for Cu, Cu_2O, CuO, and $Cu(OH)_2$ appear in the 912–922 eV range [45] (in particular at 919.0, 916.7, 918.2 and 916.3 eV for Cu, Cu_2O, CuO and ($Cu(OH)_2$ + Cu_2O), respectively) and according to Nefedov et al. [46], the contribution due to $Cu(NO_3)_2$ appears at 915.1 eV [47]. Fig. 2 shows that in this interval, the signal intensity for the P25-Cu samples is higher than for P25. The following observations can be outlined:

For sample P25-Cu-i there are maxima at about 915 and 917 eV which suggest the presence of $Cu(NO_3)_2$, $Cu(OH)_2$ and of Cu_2O. For P25-Cu-ic, maxima at about 915 and 918 eV probably correspond to Cu_2O and CuO. It must be also mentioned that the main peak is shifted by 0.51 eV to lower values with respect to the position in P25 (921.92 eV), indicating a stronger Cu-Ti interaction. This analysis allows confirming that peak A in the XPS data of these two samples (Fig. 1b) does not correspond to Cu(0).

For P25-Cu-ich, the Auger signal also shows the features commented for P25-Cu-ic, but the contribution at 919 eV reveals that this sample contains Cu(0). In this case, the shift of the main signal to lower values is 0.15 eV.

The Auger profile of sample P25-Cu-ib is very similar to that of P25 with an additional contribution at 916 eV that can correspond to Cu_2O and/or $Cu(OH)_2$ species. Finally, for P25-Cu-o the profile is very similar to that of P25 due to the low surface Cu content.

In addition to the above interpretation, it must be considered that copper is coordinated not only to oxygen forming copper oxides, but also to oxygen and/or titanium from the P25 surface which can influence the electronic and structural characteristics of the supported species.

Figure S5 shows the O1s XPS data. For P25, the main peak is due to O-Ti (529.5 eV, TiO_2 lattice oxygen) and the shoulder includes two contributions: at 531 eV, corresponding to O in surface OH groups (Ti-O-H species) and at 532.4 eV, probably due to adsorbed H_2O [48]. Precise B.E. values are shown in Table S5. In general, the same features are observed for the P25-Cu samples, although the main peak is somewhat

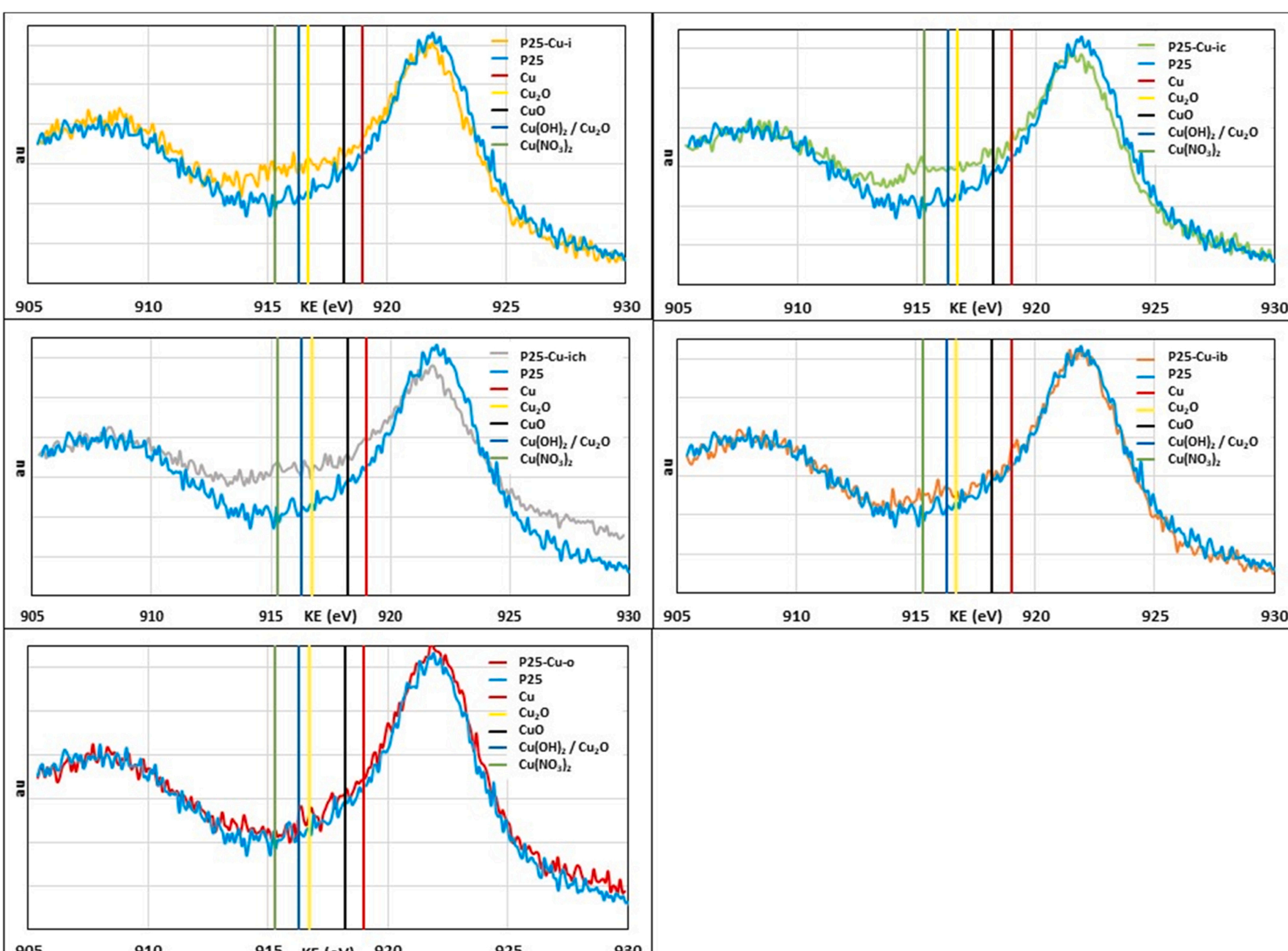

Fig. 2. Auger spectra of each P25-Cu photocatalyst compared to that of P25 (B.E. of the main maximum and the corresponding electrons kinetic energy energy (K.E.) are shown in Table S4).

shifted to higher B.E., probably due to the interaction of oxygen with Cu species. The magnitude of this shift slightly varies for the different P25-Cu samples, being higher for samples treated (calcined and/or reduced) at higher temperature. A similar shift has been observed in the Ti2p XPS analysis (Figure S6). The main peak is slightly shifted to higher B.E. values in the P25-Cu catalysts with respect to P25. This means either that copper species interact with O and Ti atoms in a similar way and/or that a certain distortion of the outer TiO_2 surface structure occurs upon copper incorporation. The largest effect is found for samples P25-Cu-ic and P25-Cu-ich (treated at 500 °C), for which the amount of surface Cu is higher than for the rest of the samples. This indicates that copper does not diffuse in the TiO_2 bulk and, thus, the commented XPS shifts are due to modifications occurring in a very external position, close to the surface.

In the case of the P25-Cu-i sample, the relatively intense peak at about 532 eV can be attributed to the presence of NO_3^- (O1s B.E. 532.5–533.6 eV). The O 1s XPS profiles of samples P25-Cu-ic, P25-Cu-ich and P25-Cu-ib do not show this peak, indicating that nitrates have been completely removed by the heat treatments. For P25-Cu-o, the relatively intense contribution at 531.3 eV is probably related to the remaining oxalate or acetate species [48]. The N1s analysis shows for sample P25-Cu-i a peak at 406.71 eV, characteristic of NO_3^- species [47, 49], confirming the presence of nitrates (about 0.92 wt% N) in it and the absence in the rest of samples (Figure S7).

3.1.5. TEM results

The obtained TEM images are shown in Figure S8. Sample P25-Cu-i (Figure S8a (image also shown in Fig. 3a)) contains very well dispersed particles all over the surface. As it has been prepared in mild conditions, the formation of metal or metal oxide clusters is not expected. According to the aspect of this sample (Figure S3), the observed particles could be copper basic salts formed by the interaction of the $Cu(NO_3)_2$ solution with the TiO_2 surface. In samples P25-Cu-ic and P25-Cu-ich, Cu particles are visible and well dispersed, but larger (Figures S8b and S8c), likely due to sintering associated with the thermal treatment. They could be Cu_2O and/or CuO in P25-Cu-ic and Cu(0) and/or Cu_2O in P25-Cu-ich. Since the reduction treatment can lead to the migration of partially reduced titanium oxide towards copper particles producing the SMSI (Strong Metal-Support Interaction) effect, Cu particles might be covered by titania or a Cu-Ti alloy can be formed (as reported for Ru supported on ZnO [50]).

Very few particles are observed for P25-Cu-ib (Figure S8d), in agreement with the lower Cu loading. The TEM images of the P25-Cu-o catalyst show larger particles (and closer together) that might be also covered by sodium species (Figure S8e), suggestion supported by the large amount of superficial Na detected by XPS.

The proposed copper species present in each catalyst and the estimated particle size are shown in Table S6.

3.2. Photoreforming of cellulose

Fig. 3b shows the hydrogen generation (μmol·gcat^{-1}) vs time recorded for all the tested photocatalysts. The analogous data of CO_2 generation are presented in Figure S9.

The amount of generated H_2 and CO_2 (in μmol·h^{-1}·g$_{cat}^{-1}$) is presented in Table 1. Blank B2 renders 2.6 μmol H_2 and 18.3 μmol CO_2, while in blank B1, the production of H_2 and CO_2 is 2.1 and 0.7 μmol, respectively, showing that cellulose photooxidation and water photolysis are negligible.

Data in Table 1 show that all the P25-Cu catalysts are more active than bare P25. The largest amount of H_2 (in μmol·h^{-1}·g$_{cat}^{-1}$) is produced using the P25-Cu-i catalyst, followed by P25-Cu-ib, while the less active samples are those that have been thermally treated (calcined and/or reduced with H_2). This is in line with the recent study published by Schubert et al. [29] who considered this finding surprising. Besides, it should be noted that for the two catalysts that produce the highest amount of hydrogen, the H_2/CO_2 ratio is close to 2, which agrees with the stoichiometry of the reaction (Eq. 1).

To explain the differences between catalysts it is necessary to consider both, the nature of the Cu species present and their particle size. It is intriguing that the two most active samples, P25-Cu-i and P25-Cu-ib, have been prepared by different procedures and they contain, as-prepared, different copper species that are either active or become activated under the reaction conditions. This second option seems to be relevant for sample P25-Cu-i (as-prepared it still contains nitrate ions).

Analysis of the used catalysts should shed light on this but, unfortunately, the used catalyst is mixed with the unreacted cellulose and it is not possible to analyse it separately.

In any case, it is clear that several redox reactions will occur involving the photocatalysts components. That is, when a TiO_2-Cu photocatalyst is irradiated with light of the suitable wavelength, e^-/h^+ pairs are generated and the electrons can move towards the supported Cu species and produce potential reduction reactions, what can activate

Table 1
Results of cellulose photoreforming for the catalysts studied.

	Gas products (μmol·h^{-1}·g$_{cat}^{-1}$)		
Catalyst	H_2	CO_2	H_2/CO_2
P25	297	211	1.41
P25-Cu-i	731	407	1.80
P25-Cu-ic	437	277	1.58
P25-Cu-ih	510	313	1.63
P25-Cu-ich	470	275	1.71
P25-Cu-ib	653	341	1.92
P25-Cu-o	549	476	1.15
Blank B3a*	69	19	3.63
Blank B3b*	53	46	1.15

* see the text

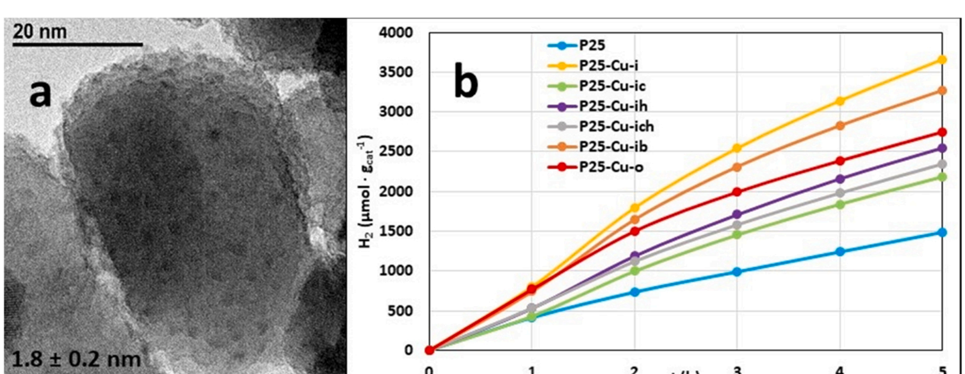

Fig. 3. a) TEM image of sample P25-Cu-i and b) Hydrogen production vs time in the photoreforming of cellulose.

the co-catalyst. If Cu(0) is formed, it would be a proper conductor of electrons to reduce H^+. If CuO is present on the TiO_2 surface, the electron transfer to the co-catalysts is feasible according to the work function values (5.9 ± 0.1 eV and 5.4 ± 0.2 eV for CuO and TiO_2, respectively) [51,52]. Such a transfer could result in the formation of Cu_2O or even Cu (0) species, and they would deliver electrons for the reduction of H^+ to H_2 and become oxidized and ready for a new electron transfer. This comment intends to point out that complex and multiple redox processes can occur on the P25-Cu photocatalysts and the obtained results show that they are more effective when the photocatalysts have not been heat-treated and the particle size of the copper species is smaller.

To better appreciate the significance of the obtained results, they have been compared with those previously published, using cellulose as sacrifice substrate and photocatalysts prepared with commercial titania (Table S7 and associated comments). Assuming that comparison of results is usually difficult due to differences in the catalyst nature, the experimental conditions, and the setup used, it can be concluded that:

- In general, the production of CO_2 is not reported in most published studies, and this is an important aspect of the process that should be also presented.
- Comparing systems that use similar power radiation, the present study gives the highest H_2 generation, and this good result is obtained with non-noble metal-based photocatalysts.

In summary, the incorporation of copper to P25 and the conditions used in this study allow the efficient hydrogen production by cellulose photoreforming. The simplest preparation method has led to the most active catalyst, meaning that this procedure leaves the catalysts in the most suitable form to become efficiently activated during their management and/or under reaction conditions.

4. Conclusions

P25-Cu catalysts prepared by different procedures have led to different supported copper species. They are significantly more active than bare P25 for the generation of hydrogen by cellulose photoreforming. The just impregnated catalyst (P25-Cu-i) and the one reduced with $NaBH_4$ at room temperature (P25-Cu-ib) show the highest activity due either to the preservation of the surface TiO_2 structure and/or to the presence of copper species more active or able to be activated in their use. Calcination and reduction heat treatments reduce the catalyst effectivity. Sample P25-Cu-i, standing out for the simple preparation method, can be considered very promising to boost the cellulose photoreforming process for obtaining green hydrogen.

CRediT authorship contribution statement

Sergio Belda Marco: Methodology, Validation, Formal analysis, Investigation, Data curation, Writing – original draft, Writing – review and editing, Visualization **MaríaAngeles Lillo-Ródenas**: Conceptualization, Validation, Formal analysis, Resources, Writing – review and editing, Visualization, Supervision, Project administration, Funding acquisition. **MaríaCarmen Román-Martínez**: Conceptualization, Validation, Formal analysis, Resources, Writing – original draft, Writing – review and editing, Visualization, Supervision, Project administration, Funding acquisition.

Declaration of Competing Interest

The authors declare that they have no known competing financial interests or personal relationships that could have appeared to influence the work reported in this paper.

Data availability

Data will be made available on request.

Acknowledgments

This work was supported by the national and regional Spanish governments (RTI2018–095291-B-100, PID2021–123079OB-I00 project funded by MCIN/AEI/10.13039/501100011033 and by ERDF A way of making Europe (European Union) and CIPROM/2021/070) (Generalitat Valenciana) and the University of Alicante (VIGROB-136).

Appendix A. Supporting information

Supplementary data associated with this article can be found in the online version at doi:10.1016/j.cattod.2022.11.006.

References

[1] S. Fuss, W.F. Lamb, M.W. Callaghan, J. Hilaire, F. Creutzig, T. Amann, T. Beringer, W. De Oliveira Garcia, J. Hartmann, T. Khanna, G. Luderer, G.F. Nemet, J. Rogelj, P. Smith, J.V. Vicente, J. Wilcox, M. Del Mar Zamora Dominguez, J.C. Minx, Environ. Res. Lett. 13 (6) (2018) 063002.
[2] N.S. Lewis, D.G. Nocera, Proc. Natl. Acad. Sci. USA (2006) 15729–15735.
[3] L.I. Granone, F. Sieland, N. Zheng, R. Dillert, D.W. Bahnemann, Green Chem. 20 (2018) 1169–1192.
[4] X. Liu, X. Duan, W. Wei, S. Wang, B.J. Ni, Green Chem. 21 (2019) 4266–4289.
[5] I. Rossetti, ISRN Chem. Eng. 2012 (2012) 1–21.
[6] A. Speltini, M. Sturini, D. Dondi, E. Annovazzi, F. Maraschi, V. Caratto, A. Profumo, A. Buttafava, Photochem. Photobiol. Sci. 13 (2014) 1410–1419.
[7] G. Zhang, C. Ni, X. Huang, A. Welgamage, L.A. Lawton, P.K.J. Robertson, J.T. S. Irvine, Chem. Commun. 52 (2016) 1673–1676.
[8] R. Verma, J. Gangwar, A.K. Srivastava, RSC Adv. 7 (2017) 44199–44224.
[9] H. Zhang, J.F. Banfield, Chem. Rev. 114 (2014) 9613–9644.
[10] S.H. Liu, H.R. Syu, Appl. Energy 100 (2012) 148–154.
[11] S.M. Gupta, M. Tripathi, Chin. Sci. Bull. 56 (2011) 1639–1657.
[12] D. Beydoun, R. Amal, G. Low, S. McEvoy, J. Nanoparticle Res. 1 (1999) 439–458.
[13] X. Fu, J. Long, X. Wang, D.Y.C. Leung, Z. Ding, L. Wu, Z. Zhang, Z. Li, X. Fu, Int. J. Hydrog. Energy 33 (2008) 6484–6491.
[14] L. Körösi, S. Papp, I. Bertóti, I. Dékány, Chem. Mater. 19 (2007) 4811–4819.
[15] H. Park, Y.K. Kim, W. Choi, J. Phys. Chem. C 115 (2011) 6141–6148.
[16] T. Kawai, T. Sakata, Nature 286 (1980) 474–476.
[17] G. Wu, T. Chen, G. Zhou, X. Zong, C. Li, Sci. China, Ser. B Chem. 51 (2008) 97–100.
[18] A. Caravaca, W. Jones, C. Hardacre, M. Bowker, Proc. R. Soc. A Math. Phys. Eng. Sci. 472 (2016) 1–21.
[19] M. Imizcoz, A.V. Puga, Catalysts 9 (2019) 1–5.
[20] S. Abdul Razak, A.H. Mahadi, R. Abdullah, H.M. Yasin, F. Ja'afar, N. Abdul Rahman, H. Bahruji, Biomass Convers. Biorefinery (2020).
[21] L. Cano-Casanova, A. Amorós-Pérez, M. Ouzzine, M.A. Lillo-Ródenas, M.C. Román-Martínez, Appl. Catal. B Environ. 220 (2018) 645–653.
[22] A. Mills, S. Le Hunte, J. Photochem. Photobiol. A Chem. 108 (1997) 1–35.
[23] A. Amorós-Pérez, L. Cano-Casanova, A. Castillo-Deltell, M.Á. Lillo-Ródenas, M. C. Román-Martínez, Materials 12 (2019) 1–18.
[24] S. Xu, J. Ng, X. Zhang, H. Bai, D.D. Sun, Int. J. Hydrog. Energy 35 (2010) 5254–5261.
[25] H.W. Richarson, D.T. Meshri. Kirk-Othmer Encyclopedia of Chemical Technology 5th ed., 7, John-Wiley and sons, 2003, p. 770.
[26] W. Fang, M. Xing, J. Zhang, J. Photochem. Photobiol. C Photochem. Rev. 32 (2017) 21–39.
[27] M. Jung, J.N. Hart, J. Scott, Y.H. Ng, Y. Jiang, R. Amal, Appl. Catal. A Gen. 521 (2016) 190–201.
[28] G. Colón, M. Maicu, M.C. Hidalgo, J.A. Navío, Appl. Catal. B Environ. 67 (2006) 41–51.
[29] J.S. Schubert, L. Kalantari, A. Lechner, A. Giesriegl, S.P. Nandan, P. Alaya, S. Kashiwaya, M. Sauer, A. Foelske, J. Rosen, P. Blaha, A. Cherevan, D. Eder, J. Mater. Chem. A 9 (2021) 21958–21971.
[30] P.A. Desario, J.J. Pietron, T.H. Brintlinger, M. McEntee, J.F. Parker, O. Baturina, R. M. Stroud, D.R. Rolison, Nanoscale 9 (2017) 11720–11729.
[31] R. López, R. Gómez, J. Sol-Gel Sci. Sci. Technol. 61 (2012) 1–7.
[32] L. Cano-Casanova, A. Amorós-Pérez, M. Ouzzine, M.C. Román-Martínez, M.A. Lillo-Ródenas, J. Environ. Chem. Eng. 9 (2021) 1–11.
[33] L. Cano-Casanova, A. Amorós-Pérez, M.Á. Lillo-Ródenas, M.C. Román-Martínez, Materials 11 (2018) 1–18.
[34] A.A. Dubale, C.J. Pan, A.G. Tamirat, H.M. Chen, W.N. Su, C.H. Chen, J. Rick, D. W. Ayele, B.A. Aragaw, J.F. Lee, Y.W. Yang, B.J. Hwang, J. Mater. Chem. A 3 (2015) 12482–12499.
[35] G. Panzeri, M. Cristina, M.S. Jagadeesh, G. Bussetti, L. Magagnin, Sci. Rep. 10 (2020) 1–10.
[36] J. Mao, Q. Gu, D.H. Gregory, Materials 8 (2015) 2191–2203.
[37] S. Sompech, A. Srion, A. Nuntiya, Procedia Eng. 32 (2012) 1012–1018.

[38] M.C. Wu, G. Tóth, A. Sápi, A.R. Leino, Z. Kónya, Á. Kukovecz, W.F. Su, K. Kordás, J. Nanosci. Nanotechnol. 12 (2012) 1421–1424.
[39] I.M. El-naggar, E.A. Mowafy, I.M. Ali, H.F. Aly, Adsorption 8 (2002) 225–234.
[40] N.S. Mcintyre, M.G. Cook, Anal. Chem. 47 (1975) 2208–2213.
[41] B.R. Strohmeier, E. Donald, R. Leyden, Scott Field David, M. Hercules, J. Phys. Chem. 94 (1985) 514–530.
[42] J.P. Espinós, J. Morales, A. Barranco, A. Caballero, J.P. Holgado, A.R. González-Elipe, J. Phys. Chem. B 106 (2002) 6921–6929.
[43] L. Huang, F. Peng, F.S. Ohuchi, Surf. Sci. 603 (2009) 2825–2834.
[44] G. Hopfengärtner, D. Borgmann, I. Rademacher, G. Wedler, E. Hums, G. W. Spitznagel, J. Electron Spectrosc. Relat. Phenom. 63 (1993) 91–116.
[45] N.S. McIntyre, S. Sunder, D.W. Shoesmith, F.W. Stanchell, J. Vac. Sci. Technol. 18 (1980) 714–721.
[46] V.I. Nefedov, E.K. Zhumadilov, T.Y. Kopytova, J. Struct. Chem. 18 (1977) 549–553.
[47] J.F. Moulder, W.F. Stickle, P.E. Sobol, K.D. Bomben, Handbook of X-Ray Photoelectron Spectroscopy, Perkin-Elmer, 1992.
[48] C.D. Wagner, D.A. Zatko, R.H. Raymond, Anal. Chem. 52 (1980) 1445–1451.
[49] G. Latha, N. Rajendran, S. Rajeswari, J. Mater. Eng. Perform. 6 (1997) 743–748.
[50] E.V. Ramos-Fernández, J. Silvestre-Albero, A. Sepúlveda-Escribano, F. Rodríguez-Reinoso, Appl. Catal. A Gen. 374 (2010) 221–227.
[51] M.T. Greiner, Z.H. Lu, N.P.G. Asia, NPG Asia Mater. 5 (2013) 1–16.
[52] M.T. Greiner, L. Chai, M.G. Helander, W.M. Tang, Z.H. Lu, Adv. Funct. Mater. 22 (2012) 4557–4568.